Thin Solid Films 519 (2011) 7738–7749

Contents lists available at ScienceDirect

Thin Solid Films

journal homepage: www.elsevier.com/locate/tsf

# Comparative study of hydrothermal treatment and thermal annealing effects on the properties of electrodeposited micro-columnar ZnO thin films

O. Lupan [a,b,*], T. Pauporté [a,*], I.M. Tiginyanu [c], V.V. Ursaki [c], V. Şontea [b], L.K. Ono [d], B. Roldan Cuenya [d], L. Chow [d]

[a] Laboratoire d'Electrochimie, Chimie des Interfaces et Modélisation pour l'Energie (LECIME), UMR 7575 CNRS, Chimie ParisTech-ENSCP, 11 rue P. et M. Curie, 75231 Paris cedex 05, France
[b] Department of Microelectronics and Semiconductor Devices, Technical University of Moldova, 168 Stefan cel Mare Blvd., Chisinau, MD-2004, Republic of Moldova
[c] Institute of Electronic Engineering and Industrial Technologies, Institute of Applied Physics, Academy of Sciences of Moldova, 5, Academiei str, MD-2028, Chisinau, Republic of Moldova
[d] Department of Physics, University of Central Florida, 4000 Central Florida Blvd., Orlando, FL 32816, USA

ARTICLE INFO

*Article history:*
Received 19 October 2010
Received in revised form 27 May 2011
Accepted 28 May 2011
Available online 6 June 2011

*Keywords:*
Zinc oxide
Thin films
Electrodeposition
Thermal annealing
Hydrothermal treatment
Photoluminescence
X-ray photoelectron spectroscopy
Raman spectroscopy

ABSTRACT

We report a comparison of the role played by different sample treatments, namely, a low-temperature hydrothermal treatment by hot $H_2O$ vapor in an autoclave versus thermal annealing in air on the properties of ZnO films grown by electrochemical deposition (ECD). Scanning electron microscopy studies reveal a homogeneous micro-columnar morphology and changes in the film surface for the two different treatments. It is found that post-growth hydrothermal treatments of ECD ZnO films at 150 °C under an aqueous environment enhance their structural and optical properties (photoluminescence, transmission, Raman spectra, etc.) similar to thermal annealing in air at higher temperatures (>200 °C). The modifications of the structural and optical properties of ZnO samples after thermal annealing in air in the temperature range of 150–600 °C are discussed. The removal of chlorine from the films by the hydrothermal treatment was evidenced which could be the main reason for the improvement of the film quality. The observation of the enhanced photoluminescence peak at 380 nm demonstrates the superior properties of the hydrothermally treated ZnO films as compared to the films annealed in air ambient at the same or higher temperature. This post-growth hydrothermal treatment would be useful for the realization of high performance optoelectronic devices on flexible supports which might not withstand at high temperature annealing treatments.

© 2011 Elsevier B.V. All rights reserved.

## 1. Introduction

Zinc oxide is an important wide-bandgap semiconducting material with numerous applications due to its unique physical and chemical properties [1–6]. In the past decades, it was demonstrated that post-growth treatments of ZnO in different atmospheres (e.g. air, $O_2$, $H_2$, $N_2$, etc.) at high temperature can lead to a substantial improvement of its structural, electrical and optical properties. The effect of thermal annealing treatments in conventional furnaces, rapid thermal annealing, and rapid photo-thermal processing on the properties of ZnO thin films [1–8] grown on different types of rigid substrates (e.g. Si, GaN, $Al_2O_3$, glass, indium-doped tin-oxide (ITO), fluorine-doped tin-oxide (FTO), etc.) have been investigated. However, recently, an increased interest in flexible plastic substrates (FPS) has arisen due to their cost-efficiency, light-weight, robustness, and the possibility of integration in flexible electronic and optoelectronic devices (e.g. smart cards & displays, etc.) and transparent electronics with higher functionality [8–11]. Therefore, a synthesis technique and gentle post-growth treatment, compatible with FPS (which is damaged at temperatures above 180–200 °C), has to be identified. In addition, such treatments should also lead to the same improved structural and light emission properties observed for high-temperature annealed microcrystalline ZnO thin films presently used in short-wavelength optoelectronic devices, solar cells, field-effect transistors, light emitting diodes and in sensing applications [11–20].

ZnO thin films and microstructures have been synthesized by a variety of processes [13,20–22] and subsequently treated to improve their optical properties and to fabricate higher performance devices. Among these, electrochemical deposition — ECD [23,24] is a low temperature process compatible with different types of substrates, including FPS [7], known to produce highly crystalline ZnO films of excellent electronic quality [23–26]. In this context, microstructured zinc oxide can be considered as a promising active material for various cost-effective optoelectronic applications on flexible or elastic substrates [27–33].

In this work, we report the growth of ZnO micro-columnar films by an electrochemical method compatible with FPS. The zinc oxide films are formed from vertically oriented micro-columns with the *c*-axis perpendicular to the substrate. It is demonstrated that their structural and optical properties can be enhanced by performing a post-

* Corresponding authors at: UMR 7575, CNRS, Chimie ParisTech-ENSCP, 11 rue P. et M. Curie, 75231 Paris, cedex 05, France. Tel.: +33 155421239; fax: +33 155426379.
*E-mail addresses:* oleg-lupan@chimie-paristech.fr (O. Lupan), thierry-pauporte@chimie-paristech.fr (T. Pauporté).

0040-6090/$ – see front matter © 2011 Elsevier B.V. All rights reserved.
doi:10.1016/j.tsf.2011.05.072

deposition hydrothermal treatment at 150 °C under a water vapor atmosphere in an autoclave. The improvement of their structural and optical properties is significantly higher than that observed after a conventional thermal annealing (CTA) in a furnace at the same temperature in air. This post-deposition hydrothermal treatment is proposed as an alternative to enhance ultraviolet (UV) emission from ZnO films grown on flexible plastic substrates, which cannot be subjected to annealing in a furnace at high temperatures.

## 2. Experimental details

### 2.1. Electrochemical deposition

ZnO thin films were prepared by the cathodic electrochemical deposition — ECD method from a 5 mM $ZnCl_2$ (Merck, 99%) aqueous solution maintained at 70 °C or 85 °C. As supporting electrolyte, 0.1 M of potassium chloride (KCl) (Fluka 98%) was employed to ensure a good conductivity in the aqueous solution [6,7,25]. The ZnO thin film was grown on a fluorine-doped tin-oxide coated glass with a sheet resistance of 10 Ω/□. In addition, a reference sample was grown on flexible polymer-based substrate — FPS coated with indium-tin-oxide. FTO or FPS substrates were used as working electrodes (WE) in a classical three electrode cell for electrochemical deposition. A platinum spiral wire was used as the counter electrode (CE). The distance between WE and CE was 3 cm, while that between the reference electrode (RE) and WE was 3.5 cm. Before electrodeposition the FTO substrates were cleaned as reported in Ref. [6]. The only differences in the substrate preparation as compared to our previous reports [6,7] are the lack of immersion in $HNO_3$ (45%) and the use of a magnetic stirrer inside the reactor. Circulation of the electrolyte is essential for our experiments, in order to reduce concentration gradients at the electrode surfaces, to remove bubbles from the electrode, and to allow a better temperature control. FPS substrates were sequentially cleaned as is described in Ref. [7]. The pH of the solutions was initially 5.5. The electrolyte (450 ml in volume) was saturated with pure oxygen for 60 min prior to the electrolysis and the $O_2$-flow was maintained until the end of the growth process (63 min). The ZnO thin films were deposited at a constant applied potential (−1.0 V for FTO and −1.1 V for FPS), and the time dependence of the current density, $j$, was recorded (not shown). After electrodeposition, ZnO thin films were rinsed with deionized water (DI) to remove unreacted products from the surface of the films, dried in air, and cut into six pieces for the different characterization experiments reported here. Samples grown at 70 °C and 85 °C were marked as #70 and #85 (Table 1), respectively. The post-deposition hydrothermal treatment (AUT) was carried out at 150 °C in a stainless steel autoclave with a certain quantity of deionized water inside. A 100 mL Teflon inner liner was used and the sample was maintained 3 cm above the DI water surface to avoid direct contact between ZnO and water. We used two conditions of hydrothermal treatment (called AUT1 and AUT2) by adding different quantities of DI $H_2O$ (18.2 MΩ cm) in the autoclave, 4 and 15 ml, respectively. The absolute pressure in the autoclave was about $476.2\times10^3$ Pa at 150 °C according to steam tables. We have observed that placing the sample in the water for the treatment should be avoided because it resulted in a substantial morphological change with the formation of agglomerated crystallites due to ZnO dissolution–crystallization processes. The samples after AUT treatment under DI $H_2O$ vapor atmosphere were compared with those after conventional thermal annealing treatments in a furnace in air at 150 °C, 400 °C and 600 °C for 1 h. ZnO films grown at 70 °C will be compared only to as-grown, AUT1, and AUT2 samples, since the samples annealed at 150 °C, 400 °C and 600 °C have already been reported in our recent work [6].

**Table 1**
Description of the sample synthesis parameters and post-growth treatment.

| Sample grown at | Type of post-growth annealing/treatment<br>— AUT — hydrothermal treatment in an autoclave under a hot water vapor atmosphere;<br>— CTA — conventional thermal annealing in a furnace in air atmosphere. | | | | | |
|---|---|---|---|---|---|---|
| | As-Grown | AUT 1 | AUT 2 | CTA 150 °C | CTA 400 °C | CTA 600 °C |
| 70 °C/FTO | #70As-Gr | #70AUT1 | #70AUT2 | – | – | – |
| 85 °C/FTO | #85As-Gr | #85AUT1 | #85AUT2 | #85T150 | #85T400 | #85T600 |
| 80 °C/FPS | #80As-Gr | #80AUT1 | #80AUT2 | #80T150 | | |

### 2.2. Characterizations of electrochemically deposited ZnO microstructured films

Phase identification of the ECD ZnO films was done with an X-ray diffractometer (XRD) Siemens D5000 (with 40 kV and 45 mA, CuKα radiation with $\lambda=1.5406$ Å). Based on Lorentzian and Gaussian line-shapes fittings, the peak position and full width at half-maximum (FWHM) were obtained. The crystallinity of the ZnO films was estimated by determining the ratio of the integrated intensity of all XRD peaks as reported before [34], and the comparison of this ratio with the ratio obtained for commercial zinc oxide powder, for which 100% crystallinity was assumed.

The morphologies of the samples were investigated using a high-resolution Ultra 55 Zeiss field emission gun scanning electron microscope (FEG-SEM) at an acceleration voltage of 10 kV. Energy dispersive X-ray spectroscopy (EDX) analyses were realized with a Bruker Li-drift silicon detector.

The ex-situ prepared samples were subsequently transferred into an ultrahigh vacuum system (UHV) for electronic/chemical characterization. All investigations were performed in a modular UHV system (SPECS GmbH) specially designed for the preparation and characterization of nanoscaled materials. The analysis chamber is equipped with a hemispherical electron energy analyzer (Phoibos 100) and dual-anode (Al-Kα, 1486.6 eV and Ag-Lα, 2984.4 eV) monochromatic X-ray source (XR50, SPECS GmbH) for X-ray photoelectron spectroscopy (XPS). The base pressure in this chamber is $1\times10^{-8}$ Pa. In our studies, Al-Kα radiation was used. Details of the experimental procedures can be found in our previous reports [5,6].

Secondary ion mass spectrometry (SIMS) was used for the analysis of the Cl content in our samples because of its excellent sensitivity and depth resolution [6]. SIMS measurements were carried out with a Physical Electronics ADEPT 1010 quadrupole analyzer with a 3 keV $Cs^+$ primary beam at 60° from normal. The typical primary beam current was 25 nA. The primary beam was raster over a 300 μm by 300 μm area, with detection of negative secondary ions from an area of 100 μm by 100 μm at the center of the scanned area. Optical transmission and absorption have been studied according to the experimental procedures which were described in previous reports [6].

The continuous wave photoluminescence (PL) was excited by the 351.1 nm line of a Spectra Physics $Ar^+$ laser. The emitted light was collected by using a lens and was analyzed with a double spectrometer ensuring a spectral resolution better than 0.5 meV. The signal was detected by a photomultiplier working in the photon counting mode. The laser power for the PL excitation was about 15 mW in an excitation spot with the diameter of 1 mm. The samples were mounted on the cold station of a LTS-22-C-330 optical cryogenic system. Raman scattering measurements were performed at room temperature with a Horiba Jobin Yvon LabRam IR system in a backscattering configuration. A 632.8 nm line of a He–Ne laser was used for off-resonance excitation with less than 4 mW power at the sample. The instrument was calibrated to the same accuracy using silicon and a naphthalene standards.

## 3. Results and discussions

### 3.1. Structural and morphological-characterizations of ZnO thin films

The crystal structure and preferential orientation of ZnO thin films on FTO substrates were studied by XRD. Fig. 1 shows that electrodeposited ZnO films are strongly textured, with the (002) reflection dominant in the sample grown on FTO. The intensity of the peaks relative to the background demonstrates high purity of the hexagonal ZnO phase and high crystallinity of these samples. All observed Bragg reflections are consistent with the Wurtzite's structure ($P6_3mc$ space group). It can be seen that electrodeposited ZnO shows a sharp XRD main peak at ~34.4°, suggesting that the ECD growth at 70 °C and 85 °C is along the *c*-axis normal to the substrate. However, the intensity ratio $\{I_{(002)}(85\ °C)\}/\{I_{(002)}(70\ °C)\}$ is about 1.3, which confirms that films grown at 85 °C have a more prominent texture than those grown at 70 °C. Texture coefficient (TC) (see Table 2) was calculated using a procedure described in Ref.[6].

The Lotgering factor (LF) [35], as a representation of the degree of orientation of the ZnO films along the *c*-axis, has been determined from X-ray diffraction patterns. The LF calculated from the intensities of XRD peaks using the method described before [36] for the as-grown ZnO films ECD at 70 °C and 85 °C equals 0.75 and 0.9, respectively. An increase of the LF by about 10% and 9%, respectively, was observed for samples after AUT treatments. Fig. 1c shows the crystallinity of the as-grown ZnO films and post-deposition treated AUT and CTA.

From the detailed analysis of the XRD data (see Table 2 for details), one can see that the intensity of the (002) peak is dependent on the type of post-growth treatment (AUT in $H_2O$ vapor or CTA in air ambient) and on the annealing temperatures of CTA, but retains the preferential orientation with the *c*-axis normal to the substrate in all studied cases.

The samples (#85) annealed CTA in air at 150 °C, 400 °C and 600 °C, showed a slight change in the intensity of the (002) diffraction peak by ~9%, 18% and 12%, respectively, (see Table 2). The XRD patterns from CTA samples did not show any other peaks (except ZnO or FTO as indicated in Fig. 1) or changes, thus we are not showing them here to avoid repetition. The signal intensity reaches a maximum value after CTA annealing at 400 °C for 1 h as compared to the as-grown sample or CTA sample annealed at 150 °C (not shown). This implies that the crystallite quality changed by annealing at 400 °C for 1 h. However, if the annealing temperature is further increased to 600 °C, then the intensity of the (002) peak increases only by a factor of 1.12 (see Table 2) as compared to the as-grown sample #85As-Gr. These results suggest that the optimum temperature to obtain ZnO films with good quality via CTA treatments in air is 400 °C (1 h).

However, the sample (#85AUT1) grown at 85 °C and hydrothermally treated at 150 °C in water vapor medium, shows a larger change (~30%) in the intensity of the (002) diffraction peak, see Fig. 1, as compared to the as-grown one. This can be explained by the improvement of the crystallinity in sample #85AUT1 (see Fig. 1c). The latter can be attributed to changes in the Cl content of the ECD samples, as will be discussed in the following sections. The FWHM values of the (002) peak are about 0.094° for the samples ECD at 70 °C. The FWHM values of the (002) peak of ZnO films grown at 85 °C on FTO substrate are about 0.094° (Fig. 1b). A relationship between the intensity of the dominant (002) XRD diffraction peak and lattice parameters is shown in Table 2.

The lattice parameter *d* (002) in the un-strained bulk ZnO is about 2.602 Å [6], and the *d* (002) value of the as-grown ECD ZnO film at 85 °C is 2.608 Å, and after annealing at 400 °C and 600 °C is 2.601 Å and 2.603 Å, respectively. After treating the AUT2 sample, the *d*(002) is 2.602 Å, which is similar to un-strained ZnO. The lattice parameters *c* and *a* obtained using standard procedures [6] are $c=5.217$ Å and $a=3.253$ Å for sample #85As-Gr and $c=5.210$ Å and $a=3.251$ Å for sample #85AUT1 (Table 2). For comparison, the un-strained ZnO crystal lattice parameters are $c=5.207$ Å and $a=3.250$ Å [6]. Our results are within that range. The value of the *c*/*a* ratio for sample #85As-Gr was 1.604 and decreased to 1.602 for the hydrothermally treated sample #85AUT1, which is in agreement with the reported value for ZnO — 1.602 [6].

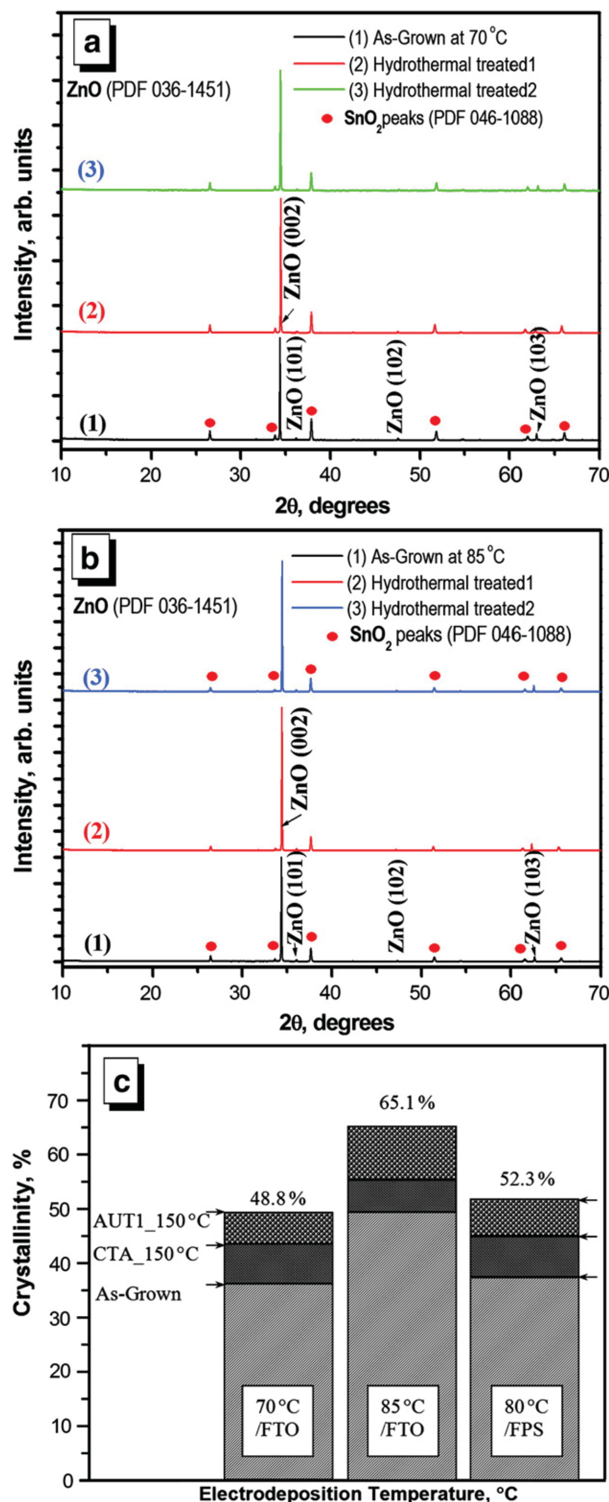


**Fig. 1.** The XRD patterns of ZnO thin films electrochemically grown on FTO at 70 °C (a) and 85 °C (b). Curve (1) denotes the as-grown sample; (2) the hydrothermally treated sample (AUT1) at 150 °C, and (3) the hydrothermally treated sample (AUT2) at 150 °C in water vapor. Representation of the degree of crystallinity of the ZnO films ECD at 70 °C, 85 °C on FTO substrates and at 80 °C on FPS and the effect of post-deposition treatment CTA or hydrothermal treatment at 150 °C (c).

**Table 2**
Effect of post-growth hydrothermal treatment in water vapor medium and thermal annealing in air on the structural properties of electrodeposited ZnO thin films.

| Type of post-growth treatment or annealing and temperature (°C) | X-ray intensity of diffraction peak (002) relative to that of as-grown films | XRD (002) peak position/degrees shift relative to that of as-grown films | *d* (Å) (002) un-stress ZnO bulk 2.602 | *a* (Å) (100) Pure ZnO 3.250 | *c* (Å) (002) Pure ZnO 5.207 | TC(002) texture coefficient-TC |
|---|---|---|---|---|---|---|
| As-grown at 85 °C | 1.00 | 34.35° | 2.608 | 3.252 | 5.217 | 3.4 |
| AUT1 150 °C | 1.29 | 34.40° (+0.05°) | 2.605 | 3.251 | 5.210 | 4.6 |
| AUT2 150 °C | 1.24 | 34.43° (+0.08°) | 2.602 | 3.255 | 5.206 | 3.5 |
| 150 °C CTA | 1.09 | 34.41° (+0.06°) | 2.603 | 3.252 | 5.207 | 3.4 |
| 400 °C CTA | 1.18 | 34.46° (+0.11°) | 2.601 | 3.252 | 5.201 | 3.8 |
| 600 °C CTA | 1.12 | 34.43° (+0.08°) | 2.603 | 3.254 | 5.206 | 3.2 |
| *#70* | | | | | | |
| As-grown at 70 °C | 1.00 | 34.35° | 2.608 | 3.255 | 5.217 | 3.2 |
| AUT1 150 °C | 1.32 | 34.43° (+0.08°) | 2.602 | 3.248 | 5.206 | 4.4 |
| AUT2 150 °C | 1.20 | 34.42° (+0.07°) | 2.603 | 3.253 | 5.207 | 3.5 |

At the same time, it is important to mention that the cell parameters from as-grown ECD ZnO films ($c = 5.217$ Å and $a = 3.253$ Å, sample #85As-Gr), demonstrate an expansion of the lattice parameter. The slightly increased '*a*' and '*c*' parameters in our samples could possibly be due to the residual Cl content and its incorporation into the structure of the ZnO structure, as was observed before for ECD films [6,22,38]. It would be expected when oxygen ions are replaced by $Cl^-$ ions because of the larger ionic radius of chlorine ($r(Cl^-) = 0.181$ nm), in comparison with those of $O^{2-}$ ($r(O^{2-}) = 0.126$ nm) and $Zn^{2+}$ ($r(Zn^{2+}) = 0.074$ nm) [6,37]. The increase in the lattice parameters could also be caused by interstitial incorporation of $Cl^-$ ions into the lattice. Similar changes of *c*-parameter were observed by Laurent et al. [38] after thermal annealing of ECD ZnO thin films prepared from a hydrogen peroxide precursor on silicon substrate. However, in our experimental results, lower values of *a* and *c* ($c = 5.210$ Å and $a = 3.251$ Å for #85AUT1) were found for ECD ZnO films hydrothermally treated in water vapor, which are very close to those of pure bulk ZnO. Also, after annealing of ZnO at 400 °C in air, the lattice constants are $a = 3.252$ Å, $c = 5.201$ Å. This suggests that hydrothermal treatment in $H_2O$ vapor affects the Cl content in the ZnO thin films, which can be one of the factors leading to the improvement of the crystal quality.

According to our previous data [6,23], a larger lattice deformation was evidenced in ECD ZnO films grown at low temperature (70 °C) as compared to samples ECD grown at 85 °C. From SEM images we could not detect significant morphological changes in the as-grown and annealed samples in air or $H_2O$ vapor. However, calculations revealed slight changes in lattice parameters (Table 2). It was observed that the crystallinity of the as-grown ZnO films increased from 37.8% to 46.0% when the corresponding ECD growth temperature was raised from 70 °C to 85 °C (Fig. 1c). The crystallinity of samples was improved in a greater degree by the AUT treatment as compared to the conventional thermal annealing at 150 °C (see Fig. 1c).

In the EDX spectrum (not shown) of ZnO films electrodeposited on a FTO substrate, features of Zn and O peaks from the ZnO film, as well as Sn from the substrate (F:$SnO_2$) were detected. The incorporation of chlorine in the ZnO films was confirmed by EDX spectra, demonstrating the presence of residual chlorine in the ZnO thin films electrodeposited from a chloride medium. The chlorine content in the as-grown zinc oxide thin films (grown at 70 °C) is about 3%, which is in agreement with previously reported values [23]. A lower Cl content (2.2%) was obtained in samples grown at 85 °C.

The effect of annealing on the [Cl]:[Zn] ratio was estimated by EDX for the ECD ZnO thin film. After sample annealing at 400 °C and 600 °C, the chlorine signal in the EDX spectra decreased while it remained constant in the titration method. According to the EDX results, thermal annealing at 400 °C in air contributes to evaporation of about 20% of Cl [6]. However, for samples hydrothermally treated at 150 °C (12 h) in an atmosphere of $H_2O$ vapor, the Cl content was decreased significantly as compared to as-grown or air-annealed samples (2 and 1.5, respectively). These data correlate with XRD results (Fig. 1) and the lattice parameter values reported above. The position of the (002) peaks of the annealed samples shifts towards higher angles as compared to those of the as-grown samples. After hydrothermal treatment the (002) peaks shift (see Table 1), showing a decrease of the lattice parameters as compared to the as-grown ZnO films, which can be correlated with the rearrangement of the atoms in the lattice and the elimination of a large quantity of Cl ions from ZnO in water vapor. This result may provide indirect evidence that chlorine is incorporated into the crystal structure, causing the as-grown ZnO crystal lattice to expand. Similar evidence was reported before [39], suggesting that the chlorine ions likely substitute oxygen in ZnO.

FEG-SEM studies were used to monitor the surface morphology of the as-grown ZnO films and the role played by the different annealing treatments. It can be seen that ZnO crystals fully cover the FTO substrates (Fig. 2).

According to the top-view SEM images, Fig. 2, the films display a micro-columnar morphology, with the radius of hexagonal faced columns in the range 100–150 nm. These crystallites look like micro-columns with preferential *c*-axis perpendicular to the substrate surface (Fig. 2 b,e inserts). The crystal sizes were nearly the same for ZnO films before and after thermal annealing, which is in agreement with previous results for ZnO grown by chemical methods [4,6,7]. These observations are in accordance with the above XRD data. However, significant morphological changes were observed for sample #70AUT2, hydrothermally treated at 150 °C for 12 h at higher water level (top-view, Fig. 2c). Such changes were not observed for sample #85AUT2 grown at 85 °C (Fig. 2f). Some holes on the lateral faces and on top of the ZnO crystallites were detected for samples #85T400 and #85T600. These observations are similar to those reported previously [6], and could be due to Cl incorporation in the ECD ZnO thin films and its removal after CTA. However, the nano-

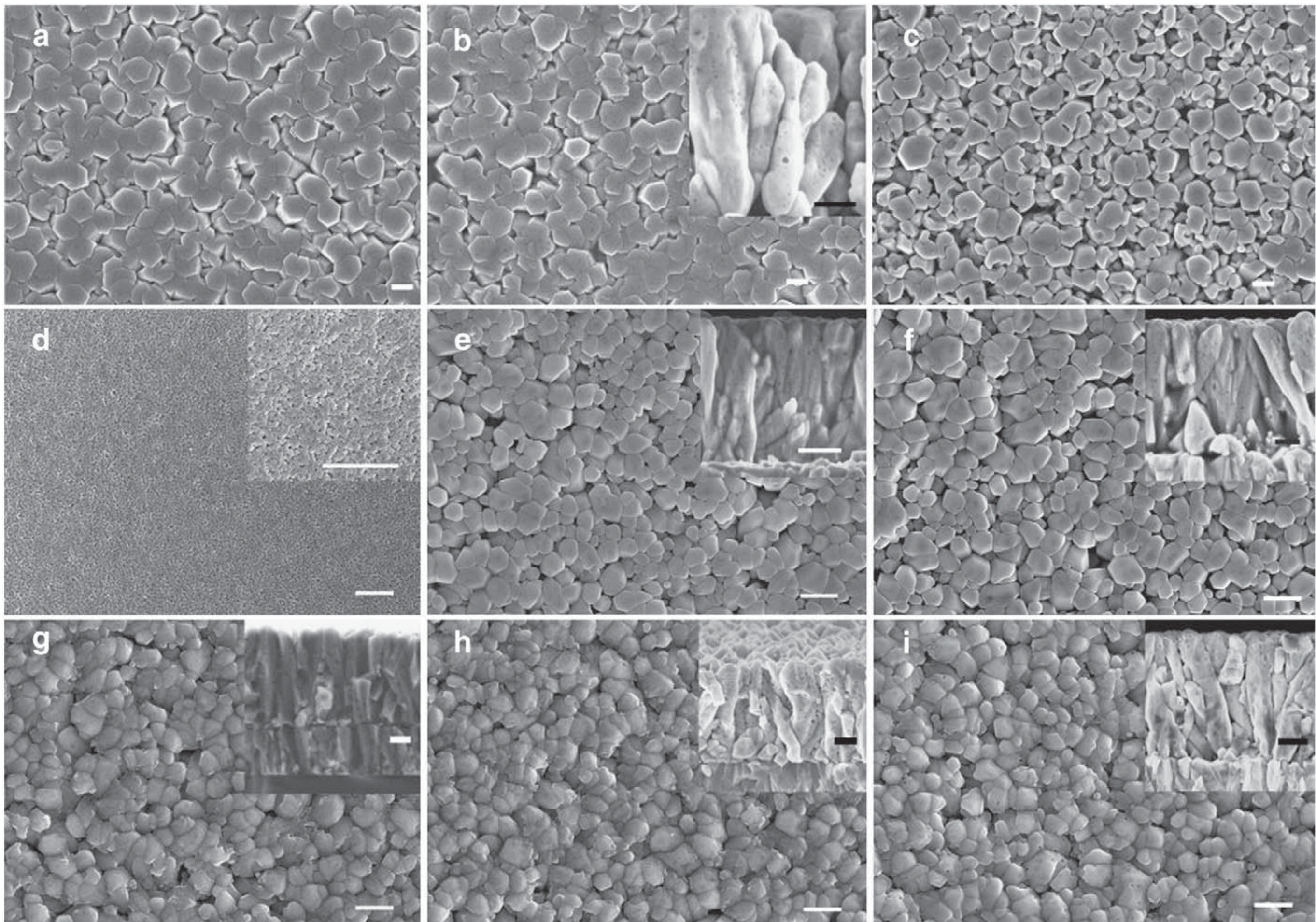


**Fig. 2.** SEM images of ECD ZnO thin films taken before and after different post-growth treatments: (a) as-grown at 70 °C; (b) AUT1, after a hydrothermal treatment at 150 °C for 12 h in $H_2O$ vapor; the insert shows a cross-sectional view of the ZnO film; (c) AUT2 after a hydrothermal treatment 12 h at 150 °C, at higher $H_2O$ level; (d) as-grown sample at 85 °C (plane view, scale bar is 5 μm); (e) AUT1 after a hydrothermal treatment at 150 °C, 12 h in $H_2O$ vapor; the insert shows a cross-sectional view of the ZnO crystallites; (f) AUT2, after a hydrothermal treatment 12 h at 150 °C, at higher $H_2O$ level; (g) sample thermally annealed in air at 150 °C for 12 h; (h) sample thermally annealed in air at 400 °C for 1 h; (i) sample thermally annealed in air at 600 °C for 1 h; the inserts in (g–i) shows a cross-sectional view of the ZnO crystallites. The scale bars are 500 nm for all images, except for (d), which is 5 μm and for all inserts are 200 nm.

holes are smaller for samples grown at 85 °C than for samples ECD at 70 °C. The nano-holes were not observed in sample #85AUT1, hydrothermally treated at 150 °C (12 h) under lower $H_2O$ level, but were seen in #85AUT2, suggesting that $H_2O$ vapor in larger quantities interacts with the ZnO surfaces and lateral grains which induce removal of ZnO and forming of nano-micro-holes.

As reported, before bulk ZnO can be decomposed at about 1950 °C [4], while for nano-ZnO this temperature is expected to be lower. Based on recent reports [4,6] there is no significant change in the sample morphology up to 800 °C. In the current work, annealing was performed at relative low temperatures (150 °C, 400 °C and 600 °C), and measurements showed that the thickness of the films remains unchanged at 1.0 μm. It is necessary to mention that the values found for the grain sizes at three different annealing temperatures are similar. The appearance of nano-holes on the surface of the films after annealing in air at temperatures higher than 400 °C could be due to the removal of incorporated chlorine in ZnO film and/or possible evaporation of chlorine-based impurities with annealing. The chlorine content in the ECD ZnO thin films seems to be a key parameter for the understanding of the observed morphological and structural changes. In this work, several techniques such as EDX, XPS and SIMS have been employed in order to better understand this issue and the distribution of Cl in the as-grown ZnO film as well as in the films annealed in air and under a $H_2O$ vapor.

### 3.2. Micro-Raman scattering

Micro-Raman scattering was used to study annealing effects on the crystal quality of ZnO films grown by ECD. Wurtzite ZnO with $C_{6v}^4$ point group symmetry demonstrates phonon modes $E_2$ (low and high frequency), $A_1$ [(TO)-transverse optical and (LO)-longitudinal optical] and $E_1$ (TO and LO), all being Raman and infrared active. Nonpolar phonon modes with symmetry $E_2$ have two frequencies, $E_{2\text{high}}$ is associated with oxygen atoms, and $E_{2\text{low}}$ is associated with Zn sublattice [6,7,20]. Raman frequencies of both polar and nonpolar optical phonons are shifted in the spectra obtained from ZnO microstructures compared to their positions in the spectra from bulk ZnO. Fig. 3 shows the Raman spectra of ZnO films ECD on FTO substrates, which were measured in backscattering geometry in the as-grown and annealed samples.

Considering the exclusion of the reference FTO substrate peaks, from both as-grown and air-annealed films, we observed three peaks related to ZnO; the characteristic and strong $E_{2(\text{high and low})}$ modes at 438–439 $cm^{-1}$ and 100 $cm^{-1}$, in addition to weak second-order $2E_2$ mode at 333 $cm^{-1}$. Fig. 3 shows clear Raman peaks indicating that different samples of ZnO films on FTO exhibit similar scattering peak, demonstrating that they have identical crystal wurtzite structures as confirmed by XRD. The higher $E_2$(high) mode peak in annealed samples indicates that the crystalline quality of the ZnO is improved

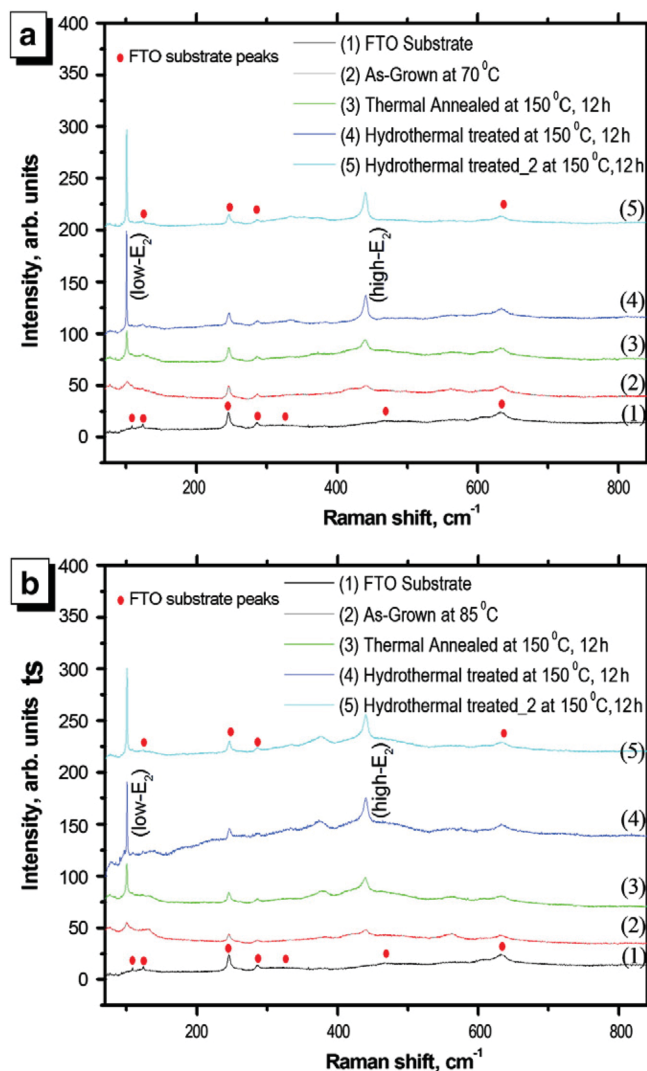


**Fig. 3.** Raman spectra for as-grown and annealed ZnO thin films on FTO substrates. Curve 1 shows Raman spectra from the FTO substrate; 2 — as-grown sample; 3 — thermally annealed at 150 °C; 4 — hydrothermally treated AUT1; and 5 — hydrothermally treated AUT2. Graphs are for ZnO films (a) grown at 70 °C and (b) grown at 85 °C by ECD.

by annealing. After annealing, the sharpness and intensity of the $E_2$ (high and low) modes and $E_1$(LO) peaks increased. The Raman spectrum of the ZnO films CTA annealed at 150 °C demonstrates the good quality of the wurtzite crystal structure in the produced material.

All samples exhibit similar scattering peaks, indicating that they have identical crystal structures as confirmed by XRD. All the scattering peaks are assigned to either ZnO or the FTO substrate. These results are in agreement with XRD and EDX data.

The intensity of the Raman peaks relative to the background demonstrates the high purity of the hexagonal ZnO phase synthesized, and the high crystallinity of the samples, which is in accordance with the above results. However, the intensity ratio of the hydrothermally treated AUT samples is larger than that of the CTA thermally annealed one, which suggests that films are of higher quality after hydrothermal treatment as compared to annealing in air. Similar results were obtained for ZnO films grown on flexible substrates.

### 3.3. Chemical characterizations (XPS and SIMS) of ZnO films

To study the effects of hydrothermal treatment on the surface composition and *Cl* concentration in ZnO thin films high-resolution XPS and SIMS measurements were carried out.

The surface composition of ZnO thin films synthesized by ECD and subsequently exposed to hydrothermal annealing treatments in $H_2O$ vapor atmosphere was investigated by X-ray photoelectron spectroscopy. The binding energy (BE) scale was calibrated using the adventitious carbon peak (C-1s) at 285 eV as reference [40,41]. In our samples, residual amounts of adventitious carbon and carbonyl compounds are unavoidable due to their exposure to air prior to the XPS measurements [42].

Fig. 4 shows XPS survey spectra of ZnO samples grown by ECD at 70 °C after several different treatments: (i) #70AUT1 and (ii) #70AUT2 subsequently hydrothermally treated at 150 °C in DI-$H_2O$ vapor; (iii) #85As-grown, a ZnO film grown by ECD at 85 °C, and (iv) the same sample as in (iii) but after a subsequent hydrothermal treatment AUT1 at 150 °C in DI-$H_2O$ vapor [#85AUT1]. For comparison, the XPS spectra of as-grown ZnO films prepared by ECD at 70 °C as well as data from an analogous sample subsequently thermally annealed in a tubular furnace in air can be found in our previous publication [6]. The following elements were detected: Zn, O, Cl, and C (adventitious). No other contaminants from the ECD process were observed. The small features at ~230 eV and ~400 eV in the survey spectrum of sample #70AUT1 (i) corresponds to the Mo-3d and Mo-3p core levels from the sample

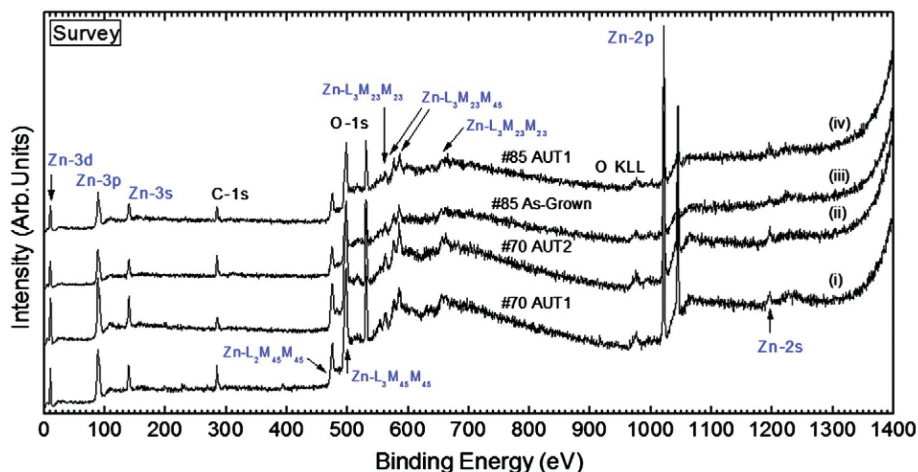


**Fig. 4.** Survey XPS spectra corresponding to ZnO films supported on FTO/glass substrates. The different photoelectron and AES peaks observed for the latter elements are labeled in the graph.

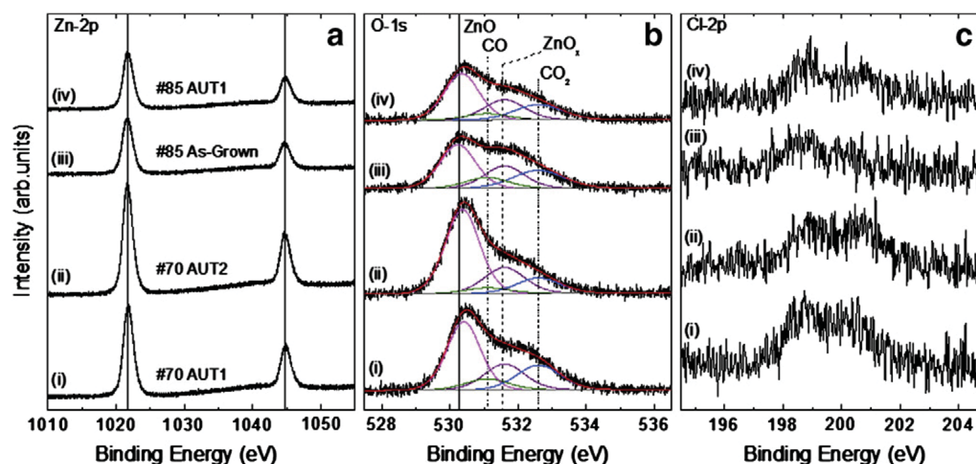


**Fig. 5.** XPS spectra (Al-$K_\alpha$ = 1486.6 eV) corresponding to the (a) Zn-2p, (b) O-1s, and (c) Cl-2p core level regions of ZnO films supported on FTO/glass substrates before (as-prepared, sample #85 As-grown) and after several hydrothermal treatments (samples #70 AUT1, #70 AUT2, and #85 AUT1).

holder that was partially exposed to the X-ray beam during the measurements.

Fig. 5 shows XPS spectra of the (a) Zn-2p, (b) O-1s, and (c) Cl-2p core level regions of our samples. The Sn-3d spectra were also recorded (not shown) and no other signals from the FTO substrate were detected by XPS. The probing depth of XPS is about 10 nm and since from the SEM images shown in Fig. 2 zinc oxide thicknesses of ~1000 nm can be inferred, no XPS signal from the underlying FTO substrate is expected. The ZnO films display a doublet at 1021.7 eV and 1044.8 eV (vertical reference lines) corresponding to the Zn-$2p_{3/2}$ and $2p_{1/2}$ core levels of ZnO, Fig. 5(a). These BEs are in agreement with previous studies from our group on ZnO films synthesized by an aqueous chemical growth route [6,40,43,44]. Although small amounts of Cl were inferred from our high-resolution XPS spectra of the Cl-2p region, Fig. 5(c), the dominant formation of Zn–O compounds is observed in these samples, since higher BEs than the ones reported above have been assigned to Zn-$2p_{3/2}$ in $ZnCl_2$ (~1023.6 eV) [6,45]. The Cl species are due to our ECD sample preparation method. In agreement with our SEM-EDX data and slight changes were detected when comparing samples exposed to different types of post-growth treatments, Fig. 5(c). The low intensities of the Cl-2p signals measured by XPS as well as the relative proximity in the BEs of the most common chlorinated Zn species ($ZnCl_2$, ZnOCl, hydroxichlorides, etc.) [46–48] prevents a specific assignment solely based on our XPS data.

The asymmetric feature observed in the O-1s region, Fig. 5(b), was deconvoluted by four subspectral components: (i) stoichiometric ZnO (530.2 eV, solid line), (ii) defective $ZnO_x$[49–52] (531.6 eV, dashed line), (iii) adventitious CO (531.1 eV, dotted line), and (iv) adventitious $CO_2$ (532.5 eV, dashed–dotted line) [53,54,55]. Table 3 shows the relative content of each Zn-containing species determined from the fits of our XPS spectra. In the O-1s region, the BE difference between stoichiometric and defective ZnO is sufficiently large to be separated, while the same distinction is not possible for the Zn-2p region due to the closer overlap of both species. Nevertheless, the large widths of the Zn-2p peaks (see Table 3, Zn-$2p_{3/2}$) also suggest the possibility of having Zn species in more than one chemical environment in these samples.

Armelao et al. [56] and Liqiang et al. [57] observed similar O-1s spectra for ZnO films and nanoparticles and attributed the high BE peak features (531.6 eV) to Zn–OH species. Considering their O-1s/Zn-2p XPS intensity ratios, the $ZnO_x(OH)_y$ stoichiometry was suggested [56]. The 531.6 eV component detected in our samples could be also attributed to the presence of $ZnO_x(OH)_y$. However, defective $ZnO_x$ (partially reduced during annealing) would also lead to a similar spectrum [49]. The as-prepared sample grown at 70 °C (#70 As-grown) shows a $ZnO/ZnO_x(OH)_y$ ratio of 1.89 [6], which was found to increase to 2.16 and 2.72 after the hydrothermal treatments of #70AUT1 and #70AUT2, respectively. By comparing the $ZnO/ZnO_x(OH)_y$ = 1.86 of a similarly prepared sample annealed in air in a furnace at 150 °C (from Ref. [6]) we can infer that the post-growth treatment in water vapor atmosphere leads to an increase in the content of stoichiometric ZnO at the expense of defective $ZnO_x$. A similar trend is observed when comparing the ZnO film grown at 85 °C (#85As-grown) to the analogous but hydrothermally treated sample (#85AUT1), with $ZnO/ZnO_x(OH)_y$ ratios of 1.72 and 1.97.

Secondary ion mass spectrometry is used for the analysis of trace elements in semiconductors and thin films, due to its exceptional sensitivity and depth profiling capability. Fig. 6 shows the $Zn^{64}$ and $Cl^{37}$ isotopic composition depth profiles in the as-grown, AUT1 and AUT2 (at 150 °C) ZnO/FTO samples measured by SIMS using the $Cs^+$ primary beam at a source potential of 3 kV and an impact angle of 60° from normal. The vertical axis shows the count rates of Zn and Cl ions in the as-deposited, hydrothermally treated and CTA annealed samples. Since no calibration standard was available, the absolute concentration of Cl ions could not be obtained from our measurements. The depth profile of Cl ions is fairly uniform for the as-deposited ZnO sample (see Fig. 6). However, after the AUT treatment, the Cl count rate of the ZnO layer grown at 70 °C is clearly reduced (Fig. 6a), indicating the removal of chlorine from ZnO and possible evaporation/removal of chlorine after hydrothermal treatment at 150 °C in water vapor atmosphere performed in an autoclave.

The SIMS results presented in Fig. 6b show that ZnO thin films grown by ECD at 85 °C possess less chlorine than samples grown at 70 °C. At the same time, Fig. 6 demonstrates that annealing at 150 °C modifies the SIMS depth profile of the ZnO films. Also, hydrothermal treatments in $H_2O$ vapor influence the chlorine content in the ZnO films grown via ECD at 70 °C or 85 °C. This might confirm the statement made based on the FEG-SEM image of Fig. 2f that the appearance of nano-holes voids on the surface of ZnO crystallites after annealing could be due to the possible evaporation/removal of chlorine-based impurities from ZnO. Also we observe that the Cl content decreased in the depth of ZnO sample. These data correlate with EDX results which show lower Cl concentration. The decrease in the Cl content may be due to the Cl removal from the lateral facets of ZnO crystals and substitution with oxygen from water vapor after hydrothermal treatment.

According to data presented in Fig. 6, the diffusion of Cl from the ZnO film into the FTO substrate at the ZnO/FTO interface is observed. This is indicated by the $Cl^{37}$ curve in the annealed sample with respect to the slope of $Cl^{37}$ in the as-grown ZnO near the interface between ZnO and FTO.

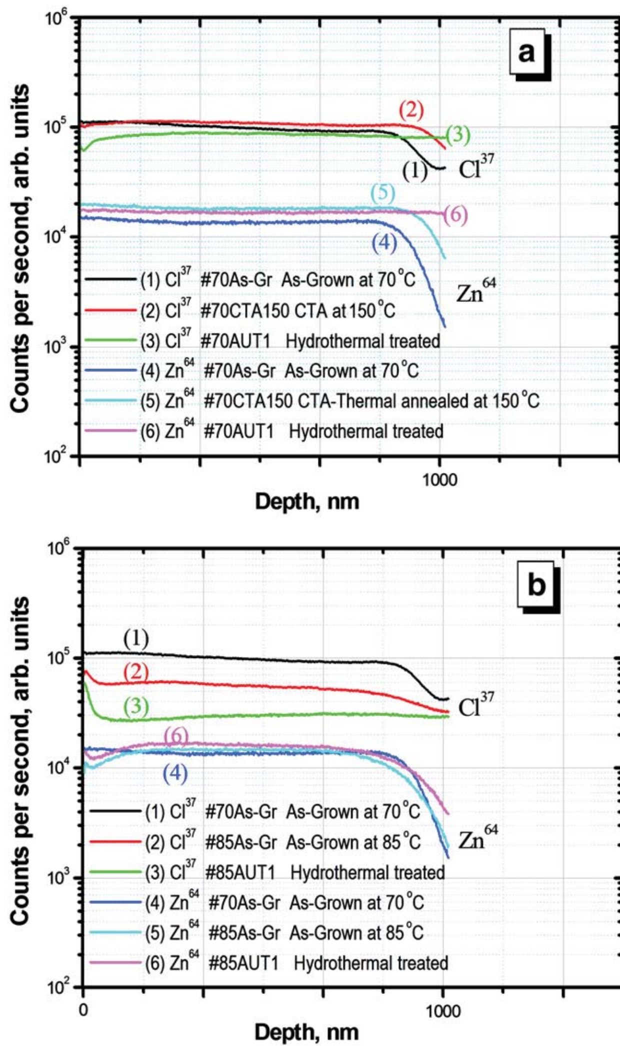


**Fig. 6.** (a) SIMS depth profiles of an as-grown ZnO film electrodeposited at 70 °C on FTO, of a film annealed at 150 °C in air (red curve on-line) and of a hydrothermally treated film in $H_2O$ vapor (green curve on-line); (b) SIMS depth profiles of as-grown ZnO film electrodeposited at 70 °C and 85 °C on FTO substrate and of hydrothermally treated ZnO in $H_2O$ vapor (green curve on-line).

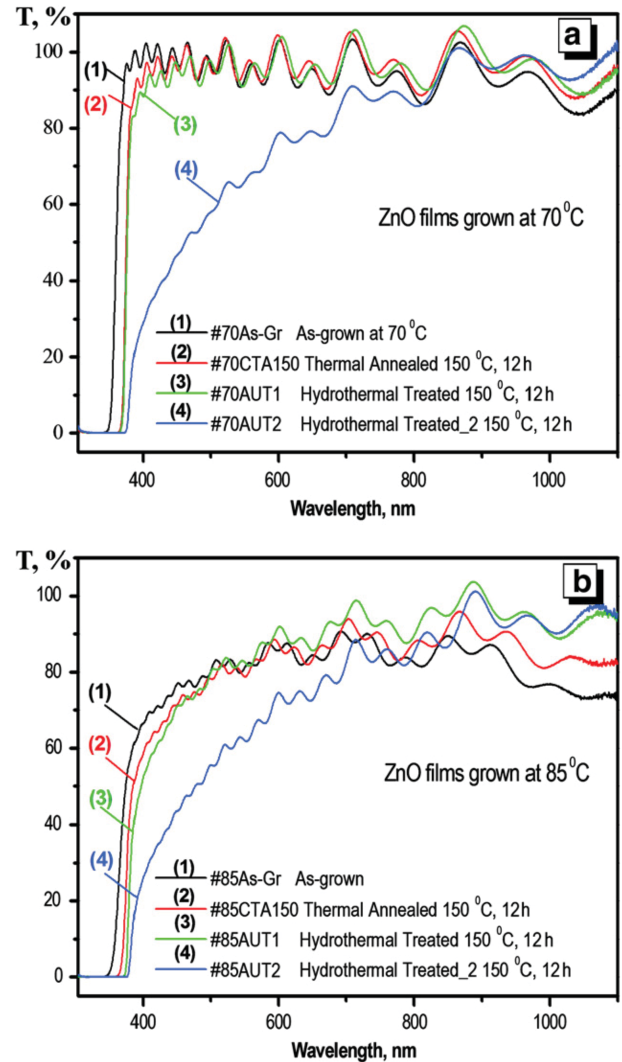


**Fig. 7.** Transmission spectra of ZnO thin films electrochemically grown on FTO substrates at 70 °C (a) and at 85 °C (b). Curves denote: (1) as-grown sample; (2) thermally annealed at 150 °C in furnace in air ambient, (3) hydrothermally treated sample (AUT1) at 150 °C and (4) hydrothermally treated sample(AUT2) at 150 °C in $H_2O$ vapor atmosphere, respectively.

### *3.4. Optical characterizations of ZnO films*

Fig. 7 shows optical transmittance spectra of as-grown ZnO thin films, thermally annealed or hydrothermally treated at 150 °C in air and hot $H_2O$ vapor, respectively. The interference fringes indicate that all of the ZnO films have optically smooth surfaces and that the interface with the FTO substrate is also smooth [6,58]. Four characteristic spectra of ZnO films in the wavelength range 300–1100 nm (Fig. 7a) are labeled as (1)–(4) for the as-electrodeposited, thermally annealed at 150 °C and hydrothermally treated films at 150 °C (regimes 1-AUT1 and 2-AUT2), respectively. All films ECD at 70 °C exhibit a high transparency (over 90%) in the visible range of the spectra and in the UV region, the optical transmittance falls sharply due to the onset of the fundamental absorption in this region. It can be seen that the optical transmittance spectrum of the ZnO sample is characteristic of the pure ZnO phase with a fundamental absorption edge observed at ~3.4 eV, which corresponds to the optical bandgap edge ($E_g$) for crystalline zinc oxide. This is important for applications in optoelectronic devices, transparent conductive films, and solar cell windows. By comparing transmission spectra curves (1) and (2) in Fig. 7 corresponding to the as-grown and CTA annealed samples, a shift in the absorption edge can be observed. The transmittance was found to change in the visible region, decreasing in the UV region with increasing annealing temperature. For the film annealed at 150 °C (curve (2), Fig. 7a), the optical transmittance (T>95%) in the visible region increases by ~4% as compared to with the as-grown ECD ZnO thin film (curve (1)). Similar effects were observed for sample #70AUT1. However, sample #70AUT2 which has been hydrothermally treated at higher DI water in the autoclave shows lower transmittance characteristics. These results correlate with SEM data in Fig. 2c demonstrating changes in the surface morphology of the films. Fig. 7 demonstrates that the absorption edge shifted to longer

**Table 3**
Relative content of stoichiometric ZnO, defective ZnOx and/or ZnOx(OH)y as well as adventitious CO and $CO_2$ species obtained from the analysis (spectral area) of the O-1s core level region of ZnO films exposed to different treatments.

| Sample | ZnO (at.%) (530.2 eV) | $ZnO_x$ or $ZnO_x(OH)_y$ (at.%) (531.6 eV) | CO (531.1 eV) | $CO_2$ (at.%) (532.5 eV) |
|---|---|---|---|---|
| (i) #70AUT1 | 46.5 | 21.5 | 22.0 | 10.0 |
| (ii) #70AUT2 | 59.3 | 21.8 | 13.7 | 5.2 |
| (iii) #85As-Gr | 40.2 | 23.3 | 24.0 | 12.5 |
| (iv) #85AUT1 | 47.0 | 23.9 | 20.9 | 8.2 |

wavelength after the two types of post-growth treatments. For the films grown at 70 °C or 85 °C and the samples hydrothermally treated at 150 °C in regime 2(AUT2), the optical transmittance in the 380–700 nm region decreases by ~30–40% compared with that of film CTA annealed at 150 °C. The latter effect is probably due to the surface roughness increase observed on these samples (Fig. 2c and f).

The optical absorption coefficient was evaluated as described previously in Ref. [6]. The functional dependences of $(\alpha h\nu)^2$ versus photon energy ($h\nu$) are presented in Fig. 8. The photon energy depends on the absorption coefficient $\alpha$ near the ultraviolet (UV) edge of the ECD ZnO films as shown in Fig. 8a.

Although the transmission in the transparent region did not show large changes (about 5–10%), the absorption edge was shifted toward a longer wavelength of about 9.8 nm (98 meV) by annealing ZnO(grown at 85 °C) at 150 °C in air and of about 12 nm (120 meV) for the hydrothermally treated sample at 150 °C in $H_2O$ vapor medium, respectively. As can be seen in Fig. 8 the amount of the shift depends on the type of post-growth treatment and may be attributed to the annealing of intrinsic and extrinsic defects (chlorine possibly being one of them). The high energy band gap of the as-grown ZnO films in the chloride medium has been assigned to a Burstein–Moss effect, the high value being due to doping [6,23]. The annealing of defects by thermal treatment induces a decrease in donor concentration and the shift of energy band gap towards lower values. It is expected that with increasing annealing temperature, the stoichiometry of the films will be improved and the defect density decreased [6,59]. The evaporation/removal of *Cl* may be the way to decrease the donor concentration after the hydrothermal treatment in hot $H_2O$ vapor.

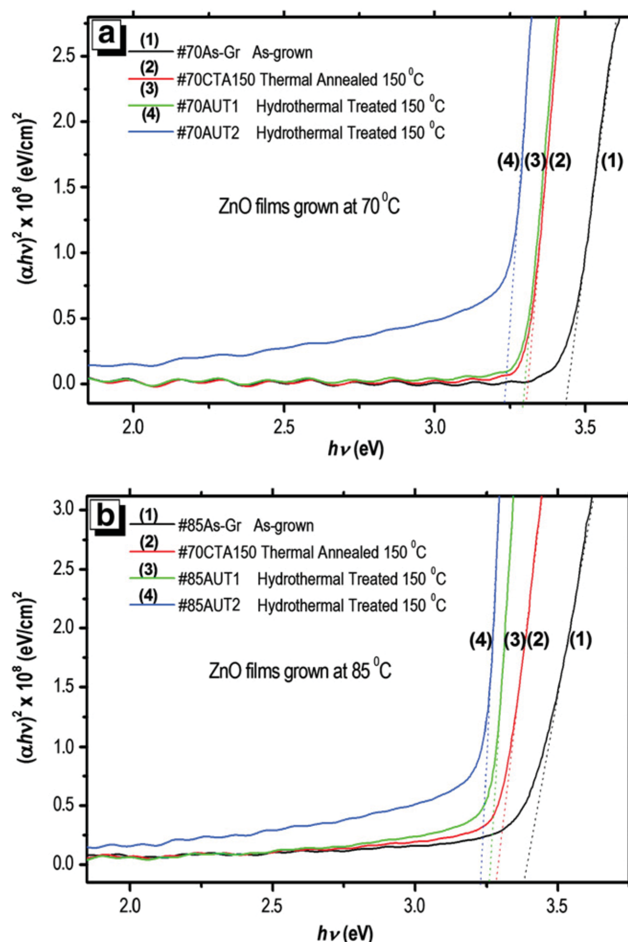


**Fig. 8.** Plot of $(\alpha h\nu)^2$versus photon energy ($h\nu$) for as-grown ZnO film electrodeposited at: (a) 70 °C and (b) 85 °C on FTO substrates. Curves denote: (1) as-grown sample; (2) thermally annealed at 150 °C in furnace in air, (3) hydrothermally treated sample (AUT1) at 150 °C and (4) hydrothermally treated sample(AUT2) at 150 °C in $H_2O$ vapor atmosphere, respectively. Also shown is the slope of the linear fit from linear region of this plot.

### 3.5. Photoluminescence of ZnO films

The photoluminescence (PL) spectrum (Fig. 9) of the as-grown sample at 85 °C consists of a broad near bandgap band with a wing at photon energies higher than the ZnO bandgap. This wing may be either due to the Burstein–Moss effect in a heavily doped ZnO sample or due to the variation of the material bandgap caused by the deviation from the stoichiometry (presence of hydroxide) according to the XPS data presented above.

Thermal annealing of the sample at 150 °C in air leads to the disappearance of the high energy wing, and to the narrowing of the PL band. Nevertheless, the PL remains still broad enough, and exhibits an asymmetric shape with a pronounced tail in the region of low photon energies. Similar characteristics of the near bandgap luminescence have been previously observed in highly doped ZnO samples grown by different methods [4,60–62]. It was shown that this PL band is likely due

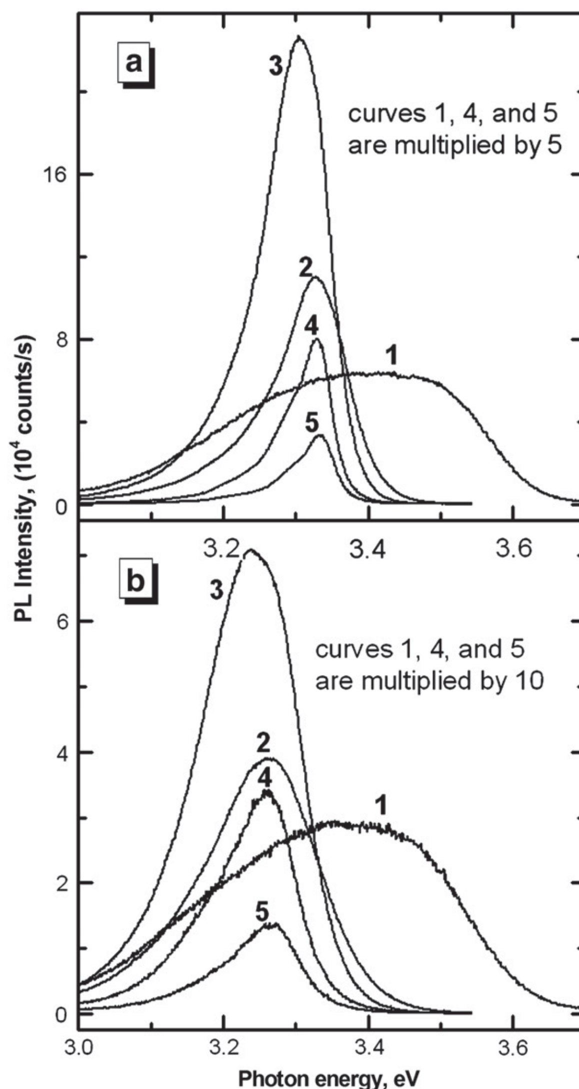


**Fig. 9.** Near bandgap PL spectrum of the as-grown sample #85As-Gr (curve 1), the sample (#85T150) thermal annealed at 150 °C in air (curve 2), the sample (#85AUT1) subjected to the hydrothermal treatment in water vapor (curve 3), the sample (#85T400) thermally annealed at 400 °C in air (curve 4), and the sample (#85T600) thermally annealed at 600 °C in air (curve 5) measured at T = 10 K (a) and T = 300 K (b).

to direct transitions of electrons between the conduction to valence band tails. The broadening of the PL band involved can be accounted for by the broadening of the band edges due to potential fluctuations induced by the high concentration of intrinsic defects or impurity in the material.

The width of the band tails, and the dependence of the FWHM of the PL band on carrier concentration can be calculated using a model for broadening of impurity bands in heavily doped semiconductors developed by Morgan [63]. By using the established dependence of the FWHM of the PL band on carrier concentration [4,60–62], one can estimate the electron concentration in our samples. These data determined at different temperatures for the as-grown sample #85As-Gr, as well as for this sample subjected to different thermal and hydrothermal treatments are presented in Table 4. The carrier concentration data for the as-grown sample #85As-Gr are not presented in this table, since the Morgan model is not applicable to this sample. As mentioned above, the Burstein–Moss effect, or the variation of the material bandgap caused by the deviation from the stoichiometry is responsible for the shape of the PL band in this case.

Note that annealing at 150 °C leads to the increase of the PL intensity by almost one order of magnitude. The hydrothermal treatment of the sample in hot water vapor results in a further narrowing of the PL band and an increase of the intensity compared to samples thermally annealed at 150 °C in air (see Fig. 9 and Table 4). These results demonstrate superiority of AUT treatment versus CTA at 150 °C to improve optical properties of ZnO micro-columnar films.

Thermal annealing of the sample #85 at 400 °C and 600 °C in air leads to a further decrease of the PL bandwidth (Fig. 9 and Table 4). However, simultaneously, the CTA annealing in air ambient leads to the decrease of the PL intensity, so that the PL intensity for the sample annealed at 400 °C is comparable with that of the as-grown sample, while the PL intensity for the sample annealed at 600 °C is even lower. One can see from Table 4 that various post-growth treatments result in the variation of the free carrier concentration at low temperatures from $6\times10^{19}\,cm^{-3}$ to $2\times10^{20}\,cm^{-3}$. Regarding the microscopic origin of the impurity, one can assume that it is related to the Cl dopant revealed by the EDX, XPS and SIMS measurements. However, the contribution of other residual impurities, i. e. H which is a shallow donor [64], cannot be withdrawn. As concerns the possible contribution related to the deviation from stoichiometry, oxygen vacancies and zinc interstitials are the most probable donor-type intrinsic defects [65,66]. Oxygen vacancies are deep donors, while zinc interstitials are not stable at room temperature and so are unlikely to contribute to the carrier concentration [67]. More complex centers involving intrinsic defects could potentially be shallow donors. However, this subject needs additional investigations.

No visible emission is observed in the as-prepared sample (Fig. 10a) as well as in the sample annealed at 150 °C (Fig. 10b). Note that the sample subjected to hydrothermal treatment also does not exhibit visible emission. This could be due to reduction of the oxygen vacancies, chlorine content and of carrier concentration in the ZnO films. Thus, it can be reduced oxygen vacancies and traps levels in

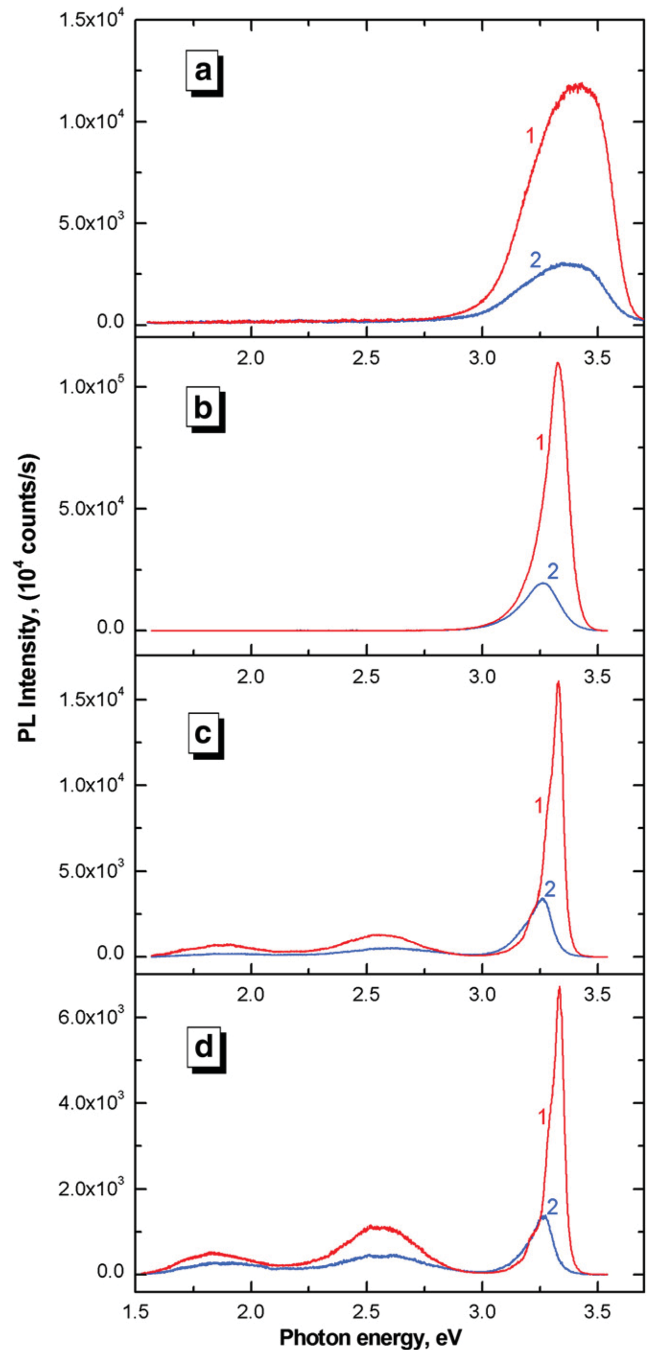


**Fig. 10.** PL spectra at ultraviolet and visible wavelengths of the sample (#85As-Gr) as-grown at 85 °C (a), and the samples annealed at 150 °C (b), 400 °C (c), and 600 °C (d) for 1 h in air. The spectra are measured at T = 10 K (curve 1), and T = 300 K (curve 2).

**Table 4**
FWHM of the near bandgap PL band, and the estimated carrier concentration in the sample #85 subjected to different treatments.

| Sample | | #85As-Gr | #85T150 | #85 AUT1 | #85T400 | #85T600 |
|---|---|---|---|---|---|---|
| T = 10 K | FWHM (meV) | 385 | 112 | 105 | 78 | 70 |
| | Carrier concentration ($cm^{-3}$) | – | $1.38\times10^{20}$ | $1.2\times10^{20}$ | $7\times10^{19}$ | $5.7\times10^{19}$ |
| T = 50 K | FWHM (meV) | 387 | 117 | 109 | 80 | 72 |
| | Carrier concentration ($cm^{-3}$) | – | $1.65\times10^{20}$ | $1.37\times10^{20}$ | $7.5\times10^{19}$ | $6\times10^{19}$ |
| T = 100 K | FWHM (meV) | 389 | 126 | 115 | 85 | 75 |
| | Carrier concentration ($cm^{-3}$) | – | $1.72\times10^{20}$ | $1.43\times10^{20}$ | $8\times10^{19}$ | $6.5\times10^{19}$ |
| T = 200 K | FWHM (meV) | 391 | 149 | 132 | 105 | 90 |
| | Carrier concentration ($cm^{-3}$) | – | $2.45\times10^{20}$ | $1.9\times10^{20}$ | $1.2\times10^{20}$ | $9\times10^{19}$ |
| T = 300 K | FWHM (meV) | 393 | 178 | 162 | 132 | 120 |
| | Carrier concentration ($cm^{-3}$) | – | $3.5\times10^{20}$ | $2.85\times10^{20}$ | $1.9\times10^{20}$ | $1.5\times10^{20}$ |

the energy band gap due to chlorine and improve the emission properties of films. At the same time, thermal annealing at 400 °C or 600 °C for 1 h in air (Fig. 10c,d) leads to the emergence of two visible PL bands at 2.55 eV and 1.85 eV. The higher the annealing temperature, the higher is the intensity of the visible emission.

The room temperature PL spectra of ZnO films grown on flexible substrates FPS as-electrodeposited (#80As-Gr), hydrothermally treated in $H_2O$ vapor (#80Aut) and thermally annealed in air at 150 °C (#80T150) are similar to samples grown on FTO. These graphs are not shown to avoid repetitions, but the main observations are described as follows. The PL spectrum of the as-electrodeposited ZnO films at 80 °C on flexible substrates exhibits a broad intensive near-band-gap band with the maximum at 380 nm (3.26 eV) at room temperature. It can be concluded that the PL spectra of the films/FPS depend significantly on annealing temperature and treatment type. The PL intensity of emission peaks increases with application of hydrothermal treatment by one order of magnitude, as well as thermal annealing by 5–6 times (not shown). The as-grown sample displays a broad spectrum covering green and yellow spectral regions. This correlates well with previous reports [6,7]. The origin of the green and yellow luminescence in ZnO is a subject of various investigations [33]. These defects could be due to ZnO surface imperfections.

Previous reports [7] have shown that excess zinc at the zinc oxide surface reacts with water vapor resulting in the release of hydrogen:

$$Zn + H_2O \rightarrow ZnO(s) + H_2(g) \quad (1)$$

It seems that the zinc in excess and other defects at the surface reacted with water vapor resulting in a smother surface of zinc oxide in our hydrothermal treatment AUT1 in an autoclave in water vapor medium. One can obtain a higher PL intensity in this way. However, the duration of hydrothermal treatment is an important factor, since the concentration of $V_{Zn}$ and $O_i$ in films increases due to the consumption of $Zn_i$ by water vapor, and the yellow luminescence emerges due to $O_i$ (not shown). However, AUT2 regime gives a rougher surface (Fig. 2c) of the ZnO films, which should be taken into account. Thus, based on our experimental results, AUT treatments can be proposed as an alternative post-growth treatment for ZnO films on flexible substrates which cannot be annealed at temperatures higher than 200 °C.

## 4. Conclusions

Since our preliminary work [7], we provide further data that hydrothermal treatment by $H_2O$ vapor atmosphere in an autoclave influences the structural, physical and optical properties of the ZnO films. Zinc oxide micro-columnar films were fabricated on rigid FTO/glass and flexible FPS substrates using a low-temperature electrochemical method. Our structural analysis revealed that the electrodeposited ZnO shows a sharp XRD main peak at ~34.4° suggesting that the growth is preferentially along the *c*-axis normal to the substrate. The narrowing of the diffraction peak width observed after thermal annealing in air is indicative of the higher crystal quality, which is further improved after the hydrothermal treatment in $H_2O$ vapor atmosphere. The hydrothermal treatment was found to induce an increase of ~30% in the intensity of the (002) XRD diffraction peak, indicating the improvement of the crystallinity of the ECD ZnO film. Raman studies of both as-grown and air-annealed ZnO demonstrate the good quality of the wurtzite crystal structure in the produced material. The intensity of the Raman peaks relative to the background demonstrates the purity of the hexagonal ZnO phase formed and crystallinity of the samples, which is in accordance with the results obtained by XRD and SEM. However, the XRD intensity ratio of hydrothermally treated AUT samples versus CTA thermally annealed one is large, which suggests that the films are of higher quality after post-growth treatment in $H_2O$ vapor compared to annealing in air ambient.

SEM studies demonstrate the same morphology for the ZnO films before and after post-growth annealing in air or in $H_2O$ vapor atmosphere. However, for one of our samples (#70AUT2), the hydrothermal treatment at 150 °C at higher $H_2O$ level leads to significant morphological changes. Such evident changes were not observed for the sample grown at 85 °C, which suggests that the ZnO films grown at 85 °C are more resilient to structural/morphological modifications. According to our EDX results, thermal annealing at 400 °C in air contributes to the elimination of about 20% of Cl [6]. However, based on SIMS results one can conclude that the Cl content was found to decrease more significantly for samples hydrothermally treated at 150 °C in $H_2O$ vapor atmosphere as compared to the thermally annealed films. XPS studies revealed that the as-prepared samples grown at 70 °C (#70 As-grown) have a $ZnO/ZnO_x(OH)_y$ ratio of 1.89 [6], which increased to 2.16 and 2.72 after the hydrothermal treatments (samples #70 AUT1 and #70 AUT2, respectively). The SIMS analysis indicated that the ZnO thin films grown by ECD at 85 °C possess less chlorine than the as-grown samples at 70 °C. At the same time, it was observed that annealing at 150 °C modifies the SIMS depth profile of the ZnO film. Also, hydrothermal treatment in $H_2O$ vapor atmosphere was found to influence the chlorine content in the ZnO films grown ECD at 70 °C or 85 °C. ZnO films grown by ECD exhibit photoluminescence (PL) spectra in the UV range. The PL spectrum of the as-prepared samples on FTO substrates consists of a broad very intensive near bandgap band with the maximum at 3.345 eV at $T = 10$ K and 3.26 eV at room temperature. No visible emission is observed in the sample (at least at the level three orders of magnitude less that the intensity of the near bandgap luminescence). Annealing at 400 °C in air leads to a significant narrowing of the near bandgap luminescence, and the emergence of two visible PL bands at 2.55 eV and 1.85 eV. The research also highlights electrodeposition of the ZnO films on flexible plastic substrates for which features of post-growth treatment are important to get a higher UV emission and improved optical properties. Thus, hydrothermal treatment in hot $H_2O$ vapor atmosphere can be an alternative to CTA in furnace for annealing of ZnO films on FPS substrates for the purpose of improving their optical properties.

## Acknowledgements

Dr. O. Lupan's post-doctoral fellowship and a part of this work were funded by C-nano Ile-de-France program (Project nanoZnO-LED). We thank Dr. S. Delpech (LECIME) for access to the Raman spectrometer. Dr. Roldan Cuenya and Dr. L.K. Ono acknowledge the financial support from the National Science Foundation (NSF DMR-0906562). Dr. L. Chow acknowledges partial financial support from USDA award #58-3148-8-175.

## References

[1] H.S. Kang, J.S. Kang, J.W. Kim, S.Y. Lee, J. Appl. Phys. 95 (2004) 1246.
[2] V. Gupta, A. Mansingh, J. Appl. Phys. 80 (1996) 1063.
[3] O. Lupan, S. Shishiyanu, V. Ursaki, H. Khallaf, L. Chow, T. Shishiyanu, V. Sontea, E. Monaico, S. Railean, Sol. Energy Mater. Sol. Cells 93 (2009) 1417.
[4] V.V. Ursaki, O.I. Lupan, L. Chow, I.M. Tiginyanu, V.V. Zalamai, Solid State Commun. 143 (2007) 437.
[5] O. Lupan, L. Chow, S. Shishiyanu, E. Monaico, T. Shishiyanu, V. Şontea, B. Roldan Cuenya, A. Naitabdi, S. Park, A. Schulte, Mater. Res. Bull. 44 (2009) 63.
[6] O. Lupan, T. Pauporté, L. Chow, B. Viana, F. Pellé, B. Roldan Cuenya, L.K. Ono, H. Heinrich, Appl. Surf. Sci. 256 (2010) 1895.
[7] O. Lupan, T. Pauporté, J. Cryst. Growth 312 (2010) 2454.
[8] A.Y.L. Sim, G.K.L. Goh, S. Tripathy, D. Andeen, F.F. Lange, Electrochim. Acta 52 (2007) 2933.
[9] A. Nadarajah, R.C. Word, J. Meiss, R. Konenkamp, Nano Lett. 8 (2008) 534.
[10] D. Pradhan, M. Kumar, Y. Ando, K.T. Leung, J. Phys. Chem. C 112 (2008) 7093.
[11] M.H. Huang, S. Mao, H. Feick, H. Yan, Y. Wu, H. Kind, E. Weber, R. Russo, P. Yang, Science 292 (2001) 1897.
[12] T. Pauporté, in: Z.M. Wang (Ed.), Toward Functional Nanomaterials, vol. 5, Springer, New-York, USA, 2009, p. 77, chap. 2, Lecture Notes in Nanoscale Science and Technology.
[13] T. Pauporté, D. Lincot, B. Viana, F. Pellé, Appl. Phys. Lett. 89 (2006) 233112.

[14] O. Lupan, T. Pauporté, B. Viana, I.M. Tiginyanu, V.V. Ursaki, R. Cortés, ACS Appl. Mater. Interfaces 2 (2010) 2083.
[15] O. Lupan, G. Chai, L. Chow, Microelectron. J. 38 (2007) 1211.
[16] O. Lupan, G. Chai, L. Chow, Microelectron. Eng. 85 (2008) 2220.
[17] G. Chai, O. Lupan, L. Chow, H. Heinrich, Sens. Actuators A 150 (2009) 184.
[18] O. Lupan, G. Chai, L. Chow, Sens. Actuators B 141 (2009) 511.
[19] T. Pauporté, G. Bataille, L. Joulaud, F.J. Vermersch, J. Phys. Chem. C. 114 (2010) 194.
[20] O. Lupan, V.V. Ursaki, G. Chai, L. Chow, G.A. Emelchenko, I.M. Tiginyanu, A.N. Gruzintsev, A.N. Redkin, Sens. Actuators B 144 (2010) 56.
[21] L. Chow, O. Lupan, H. Heinrich, G. Chai, Appl. Phys. Lett. 94 (2009) 163105.
[22] O. Lupan, G.A. Emelchenko, V.V. Ursaki, G. Chai, A.N. Redkin, A.N. Gruzintsev, I.M. Tiginyanu, L. Chow, L.K. Ono, B. Roldan Cuenya, H. Heinrich, E.E. Yakimov, Mater. Res. Bull. 45 (2010) 1026.
[23] T. Pauporté, E. Jouanno, F. Pellé, B. Viana, P. Aschehoug, J. Phys. Chem. C 113 (2009) 10422.
[24] T. Pauporté, D. Lincot, Appl. Phys. Lett. 75 (1999) 3817.
[25] T. Pauporté, D. Lincot, J. Electroanal. Chem. 517 (2001) 54.
[26] T. Pauporté, D. Lincot, J. Electrochem. Soc. 148 (2001) C310.
[27] Z.L. Wang, Mater. Sci. Eng. R 64 (2009) 33.
[28] C.Y. Lee, J.Y. Wang, Y. Chou, C.L. Cheng, C.H. Chao, S.C. Shiu, S.C. Hung, J.J. Chao, M.Y. Liu, W.F. Su, Y.F. Chen, C.F. Lin, Nanotechnology 20 (2009) 425202.
[29] M.C. Choi, Y. Kim, C.S. Ha, Prog. Polym. Sci. 33 (2008) 581.
[30] E. Fortunato, P. Barquinha, A. Pimentel, A. Gonçalves, A. Marques, L. Pereira, R. Martins, Thin Solid Films 487 (2005) 205.
[31] M. Garganourakis, S. Logothetidis, C. Pitsalidis, D. Georgiou, S. Kassavetis, A. Laskarakis, Thin Solid Films 517 (2009) 6409.
[32] C.G. Granqvist, Sol. Energy Mater. Sol. Cells 91 (2007) 1529.
[33] N. Sun, G. Fang, Q. Zheng, M. Wang, N. Liu, W. Liu, X. Zhao, Semicond. Sci. Technol. 24 (2009) 085025.
[34] G.K.L. Goh, X.Q. Han, C.P.K. Liew, C.S.S. Tay, J. Electrochem. Soc. 152 (2005) C532.
[35] B. Ma, G.K.L. Goh, J. Ma, T.J. White, J. Electrochem. Soc. 154 (2007) D557.
[36] F.K. Lotgering, J. Inorg. Nucl. Chem. 9 (1959) 113.
[37] R.D. Shannon, Acta Crystallogr. Sect. A: Found. Crystallogr. 32 (1976) 751.
[38] K. Laurent, D.P. Yu, S. Tusseau-Nenez, Y. Leprince-Wang, J. Phys. D: Appl. Phys. 41 (2008) 195410.
[39] J.B. Cui, Y.C. Soo, T.P. Chen, U.J. Gibson, J. Phys. Chem. C 112 (2008) 4475.
[40] O. Lupan, L. Chow, G. Chai, B. Roldan, A. Naitabdi, A. Schulte, H. Heinrich, Mater. Sci. Eng. B 145 (2007) 57.
[41] V. Nefedov, Y. Salyn, G. Leonhardt, R. Scheibe, J. Electron. Spectrosc. Relat. Phenom. 10 (1977) 121.
[42] K. Kawase, J. Tanimura, H. Kurokawa, K. Wakao, M. Inone, H. Umeda, A. Teramoto, J. Electrochem. Soc. 152 (2005) G163.
[43] NIST X-ray Photoelectron Spectroscopy Database, version 3.5, http://srdata.nist.gov/xps/.
[44] B.R. Strohmeier, D.M. Hercules, J. Catal. 86 (1984) 266.
[45] S.H. Jeong, D.G. Yoo, D.Y. Kim, N.E. Lee, J.H. Boo, Thin Solid Films 516 (2008) 6598.
[46] H. Matsuura, F. Tsukihashi, Metall. Mater. Trans. B 37 (2006) 413.
[47] S.W. Na, M.H. Shin, Y.M. Chung, J.G. Han, S.H. Jeung, J.H. Boo, N.E. Lee, Microelectron. Eng. 83 (2006) 328.
[48] A.E. Rakhshani, J. Phys. D: Appl. Phys. 41 (2008) 015305.
[49] Y. Tak, D. Park, K.J. Yong, J. Vac. Sci. Technol. B 24 (2006) 2047.
[50] L.C. Chao, S.J. Lin, W.C. Chang, Nucl. Instrum. Methods B 268 (2010) 1581.
[51] S. Lee, S. Bang, J. Park, S. Park, W. Jeong, H. Jeon, Phys. Status Solidi A 207 (2010) 1845.
[52] H.B. Fan, S.Y. Yang, P.F. Zhang, H.Y. Wei, X.L. Liu, C.M. Jiao, Q.S. Zhu, Y.H. Chen, Z.G. Wang, Chin. Phys. Lett. 24 (2007) 2108.
[53] K. Tanaka, K. Miyahara, I. Toyoshima, J. Phys. Chem. 88 (1984) 3504.
[54] A.F. Carley, G. Hawkins, S. Read, M.W. Roberts, Top. Catal. 8 (1999) 243.
[55] H. Onishi, C. Egawa, T. Aruga, Y. Iwasawa, Surf. Sci. 191 (1987) 479.
[56] L. Armelao, M. Fabrizio, S. Gialanella, F. Zordan, Thin Solid Films 394 (2001) 90.
[57] J. Liqiang, W. Dejun, W. Baiqi, L. Shudan, X. Baifu, F. Honggang, S. Jiazhong, J. Mol. Catal. A: Chem. 244 (2006) 193.
[58] S.T. Tan, B.J. Chen, X.W. Sun, W.J. Fan, H.S. Kwok, X.H. Zhang, S.J. Chua, J. Appl. Phys. 98 (2005) 013505.
[59] S.W. Xue, X.T. Zu, W.L. Zhou, H.X. Deng, X. Xiang, L. Zhang, H. Deng, J. Alloys Compd. 448 (2008) 21.
[60] V.V. Ursaki, I.M. Tiginyanu, V.V. Zalamai, E.V. Rusu, G.A. Emelchenko, V.M. Masalov, E.N. Samarov, Phys. Rev. B 70 (2004) 155204.
[61] V.V. Zalamai, V.V. Ursaki, E.V. Rusu, P. Arabadji, I.M. Tiginyanu, L. Sirbu, Appl. Phys. Lett. 84 (2004) 5168.
[62] E. Iliopoulos, D. Doppalopudi, H.M. Ng, T.D. Moustakas, Appl. Phys. Lett. 73 (1998) 375.
[63] T.N. Morgan, Phys. Rev. 139 (1965) A343.
[64] Y.B. Zhang, G.K.L. Goh, K.F. Ooi, S. Tripathy, J. Appl. Phys. 108 (2010) 083716.
[65] S.B. Zhang, S.H. Wei, A. Zunger, Phys. Rev. B 63 (2001) 075205.
[66] E. Oba, S.R. Nishitani, S. Isotani, H. Adachi, I. Tanaka, J. Appl. Phys. 90 (2001) 824.
[67] M.D. McCluskey, S.J. Jokela, J. Appl. Phys. 106 (2009) 071101.